

Bounds on Lorentz invariance violation from MAGIC observation of GRB 190114C

V. A. Acciari,¹ S. Ansoldi,^{2,3} L. A. Antonelli,⁴ A. Arbet Engels,⁵ D. Baack,⁶ A. Babić,⁷ B. Banerjee,⁸ U. Barres de Almeida,⁹ J. A. Barrio,¹⁰ J. Becerra González,¹ W. Bednarek,¹¹ L. Bellizzi,¹² E. Bernardini,^{13,14} A. Berti,¹⁵ J. Besenrieder,¹⁶ W. Bhattacharyya,¹³ C. Bigongiari,⁴ A. Biland,⁵ O. Blanch,¹⁷ G. Bonnoli,¹² Ž. Bošnjak,⁷ G. Busetto,¹⁴ R. Carosi,¹⁸ G. Ceribella,¹⁶ M. Cerruti,¹⁹ Y. Chai,¹⁶ A. Chilingarian,²⁰ S. Cikota,⁷ S. M. Colak,¹⁷ U. Colin,¹⁶ E. Colombo,¹ J. L. Contreras,¹⁰ J. Cortina,²¹ S. Covino,⁴ G. D'Amico,^{16,*} V. D'Elia,⁴ P. Da Vela,^{18,22} F. Dazzi,⁴ A. De Angelis,¹⁴ B. De Lotto,² M. Delfino,^{17,23} J. Delgado,^{17,23} D. Depaoli,¹⁵ F. Di Pierro,¹⁵ L. Di Venere,¹⁵ E. Do Souto Espiñeira,¹⁷ D. Dominis Prester,⁷ A. Donini,² D. Dorner,²⁴ M. Doro,¹⁴ D. Elsaesser,⁶ V. Fallah Ramazani,²⁵ A. Fattorini,⁶ G. Ferrara,⁴ L. Foffano,¹⁴ M. V. Fonseca,¹⁰ L. Font,²⁶ C. Fruck,¹⁶ S. Fukami,³ R. J. García López,¹ M. Garczarczyk,¹³ S. Gasparyan,²⁰ M. Gaug,²⁶ N. Giglietto,¹⁵ F. Giordano,¹⁵ P. Gliwny,¹¹ N. Godinović,⁷ D. Green,¹⁶ D. Hadasch,³ A. Hahn,¹⁶ J. Herrera,¹ J. Hoang,¹⁰ D. Hrupec,⁷ M. Hütten,¹⁶ T. Inada,³ S. Inoue,³ K. Ishio,¹⁶ Y. Iwamura,³ L. Jouvin,¹⁷ Y. Kajiwara,³ M. Karjalainen,¹ D. Kerszberg,^{17,†} Y. Kobayashi,³ H. Kubo,³ J. Kushida,³ A. Lamastra,⁴ D. Lelas,⁷ F. Leone,⁴ E. Lindfors,²⁵ S. Lombardi,⁴ F. Longo,^{2,27} M. López,¹⁰ R. López-Coto,¹⁴ A. López-Oramas,¹ S. Loporchio,¹⁵ B. Machado de Oliveira Fraga,⁹ C. Maggio,²⁶ P. Majumdar,⁸ M. Makariev,²⁸ M. Mallamaci,¹⁴ G. Maneva,²⁸ M. Manganaro,⁷ K. Mannheim,²⁴ L. Maraschi,⁴ M. Mariotti,¹⁴ M. Martínez,¹⁷ D. Mazin,^{16,3} S. Mender,⁶ S. Mićanović,⁷ D. Miceli,² T. Miener,¹⁰ M. Minev,²⁸ J. M. Miranda,¹² R. Mirzoyan,¹⁶ E. Molina,¹⁹ A. Moralejo,¹⁷ D. Morcuende,¹⁰ V. Moreno,²⁶ E. Moretti,¹⁷ P. Munar-Adrover,²⁶ V. Neustroev,²⁵ C. Nigro,¹⁷ K. Nilsson,²⁵ D. Ninci,¹⁷ K. Nishijima,³ K. Noda,³ L. Nogués,¹⁷ S. Nozaki,³ Y. Ohtani,³ T. Oka,³ J. Otero-Santos,¹ M. Palatiello,² D. Panequie,¹⁶ R. Paoletti,¹² J. M. Paredes,¹⁹ L. Pavletić,⁷ P. Peñil,¹⁰ C. Perennes,^{14,‡} M. Peresano,² M. Persic,^{2,29} P. G. Prada Moroni,¹⁸ E. Prandini,¹⁴ I. Puljak,⁷ W. Rhode,⁶ M. Ribó,¹⁹ J. Rico,¹⁷ C. Righi,⁴ A. Rugliancich,¹⁸ L. Saha,¹⁰ N. Sahakyan,²⁰ T. Saito,³ S. Sakurai,³ K. Satalecka,¹³ B. Schleicher,²⁴ K. Schmidt,⁶ T. Schweizer,¹⁶ J. Sitarek,¹¹ I. Šnidarić,⁷ D. Sobczynska,¹¹ A. Spolon,¹⁴ A. Stamerra,⁴ D. Strom,¹⁶ M. Strzys,³ Y. Suda,¹⁶ T. Surić,⁷ M. Takahashi,³ F. Tavecchio,⁴ P. Temnikov,²⁸ T. Terzić,^{7,§} M. Teshima,^{16,3} N. Torres-Albà,¹⁹ L. Tostí,¹⁵ J. van Scherpenberg,¹⁶ G. Vanzo,¹ M. Vazquez Acosta,¹ S. Ventura,¹² V. Verguilov,²⁸ C. F. Vigorito,¹⁵ V. Vitale,¹⁵ I. Vovk,³ M. Will,¹⁶ and D. Zarić⁷

(MAGIC Collaboration)

L. Nava^{30,31,32}

¹Inst. de Astrofísica de Canarias, E-38200 La Laguna,
and Universidad de La Laguna, Dpto. Astrofísica, E-38206 La Laguna, Tenerife, Spain

²Università di Udine, and INFN Trieste, I-33100 Udine, Italy

³Japanese MAGIC Consortium: ICRR, The University of Tokyo, 277-8582 Chiba, Japan; Department of Physics, Kyoto University, 606-8502 Kyoto, Japan; Tokai University, 259-1292 Kanagawa, Japan; RIKEN, 351-0198 Saitama, Japan

⁴National Institute for Astrophysics (INAF), I-00136 Rome, Italy

⁵ETH Zurich, CH-8093 Zurich, Switzerland

⁶Technische Universität Dortmund, D-44221 Dortmund, Germany

⁷Croatian Consortium: University of Rijeka, Department of Physics,

51000 Rijeka; University of Split - FESB, 21000 Split; University of Zagreb - FER, 10000 Zagreb; University of Osijek, 31000 Osijek; Rudjer Boskovic Institute, 10000 Zagreb, Croatia

⁸Saha Institute of Nuclear Physics, HBNI, 1/AF Bidhannagar, Salt Lake, Sector-1, Kolkata 700064, India

⁹Centro Brasileiro de Pesquisas Físicas (CBPF), 22290-180 URCA, Rio de Janeiro (RJ), Brasil

¹⁰IPARCOS Institute and EMFTEL Department,

Universidad Complutense de Madrid, E-28040 Madrid, Spain

¹¹Universidad de Lodz, Faculty of Physics and Applied Informatics,
Department of Astrophysics, 90-236 Lodz, Poland

¹²Università di Siena and INFN Pisa, I-53100 Siena, Italy

¹³Deutsches Elektronen-Synchrotron (DESY), D-15738 Zeuthen, Germany

¹⁴Università di Padova and INFN, I-35131 Padova, Italy

¹⁵Istituto Nazionale Fisica Nucleare (INFN), 00044 Frascati (Roma) Italy

¹⁶Max-Planck-Institut für Physik, D-80805 München, Germany

¹⁷Institut de Física d'Altes Energies (IFAE), The Barcelona Institute of Science and Technology (BIST), E-08193 Bellaterra (Barcelona), Spain

¹⁸Università di Pisa, and INFN Pisa, I-56126 Pisa, Italy

¹⁹Universitat de Barcelona, ICCUB, IEEC-UB, E-08028 Barcelona, Spain

²⁰The Armenian Consortium: ICRA-Net-Armenia at NAS RA, A. Alikhanyan National Laboratory

²¹Centro de Investigaciones Energéticas, Medioambientales y Tecnológicas, E-28040 Madrid, Spain

²²now at University of Innsbruck

²³also at Port d'Informaci Cientifica (PIC) E-08193 Bellaterra (Barcelona) Spain

²⁴Universität Würzburg, D-97074 Würzburg, Germany

²⁵Finnish MAGIC Consortium: Finnish Centre of Astronomy with ESO (FINCA), University of Turku, FI-20014 Turku, Finland; Astronomy Research Unit, University of Oulu, FI-90014 Oulu, Finland

²⁶Departament de Física, and CERES-IEEC, Universitat Autònoma de Barcelona, E-08193 Bellaterra, Spain

²⁷also at Dipartimento di Fisica, Università di Trieste, I-34127 Trieste, Italy

²⁸Inst. for Nucl. Research and Nucl. Energy, Bulgarian Academy of Sciences, BG-1784 Sofia, Bulgaria

²⁹also at INAF-Trieste and Dept. of Physics & Astronomy, University of Bologna

³⁰National Institute for Astrophysics (INAF), Osservatorio Astronomico di Brera, 23807 Merate, Italy

³¹Istituto Nazionale di Fisica Nucleare, Sezione di Trieste, 34149 Trieste, Italy

³²Institute for Fundamental Physics of the Universe (IFPU), 34151 Trieste, Italy

(Dated: January 28, 2020)

On January 14, 2019, the Major Atmospheric Gamma Imaging Cherenkov telescopes detected GRB 190114C above 0.2 TeV, recording the most energetic photons ever observed from a gamma-ray burst. We use this unique observation to probe an energy dependence of the speed of light in vacuo for photons as predicted by several quantum gravity models. Based on a set of assumptions on the possible intrinsic spectral and temporal evolution, we obtain competitive lower limits on the quadratic leading order of speed of light modification.

I. INTRODUCTION

At energies around the Planck energy ($E_{\text{Pl}} \approx 1.22 \times 10^{19} \text{ GeV}$), it is expected that classical quantum theory and gravity merge in a joint, yet unknown theory of quantum gravity (QG). Some candidate theories predict a violation or deformation of the Lorentz symmetry, also known as Lorentz invariance violation (LIV, [1–7]). Tiny effects of LIV could already be visible at energies much lower than E_{Pl} . One of the manifestations of LIV can be parametrized as energy-dependent corrections to the *in vacuo* photon dispersion relation

$$E^2 \simeq p^2 \times \left[1 - \sum_{n=1}^{\infty} s \left(\frac{E}{E_{\text{QG},n}} \right)^n \right], \quad (1)$$

where E and p are the energy and momentum of the photon, respectively, $E_{\text{QG},n}$ represents the QG energy scale, and s is a theory-dependent factor assuming values $+1$ or -1 . One of the consequences of a modified dispersion relation is an energy-dependent photon group velocity

$$v_{\gamma} \simeq 1 - \sum_{n=1}^{\infty} s \frac{n+1}{2} \left(\frac{E}{E_{\text{QG},n}} \right)^n, \quad (2)$$

which can be subluminal or superluminal, for $s = +1$ or $s = -1$, respectively. The consequential energy-dependent time delay between photons, taking into account only the leading LIV-correction of order n , is:

$$\Delta t = s \frac{n+1}{2} D_n(z) \left(\frac{E}{E_{\text{QG},n}} \right)^n, \quad (3)$$

where we neglect other possible energy-dependent delays due to, e.g., the intrinsic emission properties of the source, or massive photons. A modified dispersion relation would also have an effect on the $\gamma\gamma$ pair-production cross section, and thus on the absorption of γ rays [8], however in this study we focus on investigating effects on the time of flight (ToF) only. The LIV parameters

$$\eta_1 = s E_{\text{Pl}} / E_{\text{QG},1} \quad (4)$$

and

$$\eta_2 = 10^{-16} \times s E_{\text{Pl}}^2 / E_{\text{QG},2}^2, \quad (5)$$

for linear and quadratic modification, respectively, are often introduced in Eq. 3 for practicality. The information on the comoving distance between the source and the detector is included in $D_n(z)$ [9]

$$D_n(z) = \frac{1}{H_0} \int_0^z \frac{(1+\zeta)^n}{\sqrt{\Omega_{\Lambda} + (1+\zeta)^3 \Omega_m}} d\zeta, \quad (6)$$

where Ω_{Λ} , H_0 , and Ω_m denote the cosmological constant, the Hubble parameter and the matter fraction, respectively. In this work we use $H_0 = 70 \text{ km s}^{-1} \text{ Mpc}^{-1}$, $\Omega_{\Lambda} = 0.7$, and $\Omega_m = 0.3$. The systematic effect introduced by these relatively coarse values and their variations is negligible compared to the sensitivity of our analysis.

To date, the most stringent lower limits on the dispersion relation modification energy scale, resulting from ToF studies, were set using the observation of GRB 090510 with the Large Area Telescope (LAT, [10]) on board the *Fermi* satellite for the linear case, and observations of active galactic nucleus Mrk 501 with the H.E.S.S. telescopes for the quadratic case. The values are $E_{\text{QG},1} > 2.2 \times 10^{19} \text{ GeV}$ ($E_{\text{QG},1} > 3.9 \times 10^{19} \text{ GeV}$) [11] and $E_{\text{QG},2} > 8.5 \times 10^{10} \text{ GeV}$ ($E_{\text{QG},2} > 7.3 \times 10^{10} \text{ GeV}$) [12] for the subluminal (superluminal) scenario. Third class of sources used for the ToF studies on γ rays are

* Email: damico@mppmu.mpg.de

† Email: dkerszberg@ifae.es

‡ Email: cedric.perennes@pd.infn.it

§ Email: tterzic@phy.uniri.hr

pulsars. Results obtained on Crab pulsar observations with the Major Atmospheric Gamma Imaging Cherenkov (MAGIC) telescopes can be found in [13].

A possible difference in the ToF increases with the distance of the source and the energy of the photons. The sensitivity to detect the ToF effect depends inversely on the timescale of the signal variability, which provides a time reference with respect to which time delays can be looked for. Gamma-ray bursts (GRBs) are among the most distant γ -rays sources and their signal varies on sub-second timescales. As such, they were identified as excellent candidates for LIV studies many years ago [2] and already detected frequently in the high energy (HE, $E \lesssim 100$ GeV) regime with detectors on board the *Fermi* satellite [14]. However, they are notoriously difficult to detect in the very high energy (VHE, $E > 100$ GeV) band. The recent detection of GRB 190114C at redshift $z = 0.4245 \pm 0.0005$ [15, 16] with the MAGIC telescopes was the first one reported at TeV energies [17].

In this letter, we present the results of a LIV study based on the VHE γ -ray signal from GRB 190114C. The MAGIC observations and data analysis are presented in Section II. The ToF analysis applied to the GRB data is described in Section III. We present our results and discuss differences between methods in Section IV. The most important conclusions are summarized in Section V.

II. MAGIC OBSERVATION OF GRB 190114C

MAGIC is a system of two 17-meter diameter Imaging Atmospheric Cherenkov telescopes [18]. Thanks to their relatively light weight and fast repointing capability, MAGIC telescopes are optimally designed to investigate GRBs as one of their primary goals. They are located in the Roque de los Muchachos observatory on the Canary Island of La Palma at about 2200 meter above the sea level.

GRB 190114C was first detected on 14 January 2019 at 20:57:03 Universal Time (UT) (hereafter T_0) by the *Swift*-BAT [19] and the *Fermi*-GBM instruments [20]. Triggered by the alert distributed by *Swift*, the MAGIC telescopes observed GRB 190114C, detecting a strong VHE γ -ray signal [17, 21]. The data were reduced and analysed using the MAGIC Analysis and Reconstruction Software (MARS, [22, 23]). The intrinsic spectrum averaged over the time window from T_0+62 seconds to T_0+2400 seconds is well fitted with a power law function with index $\alpha = -2.5 \pm 0.2$ [21]. While the spectral slope appears to be constant for the duration of the observation, the intrinsic integrated flux in the energy range $0.3 - 1$ TeV decays as a power law with time decay index $\beta = -1.51 \pm 0.04$ [21]. This observation includes the highest energy photons ever detected from a GRB. The temporal evolution of the afterglow forward shock emission in the $0.3 - 1$ TeV energy range was modelled based on multi-wavelength (MWL) observations and theoreti-

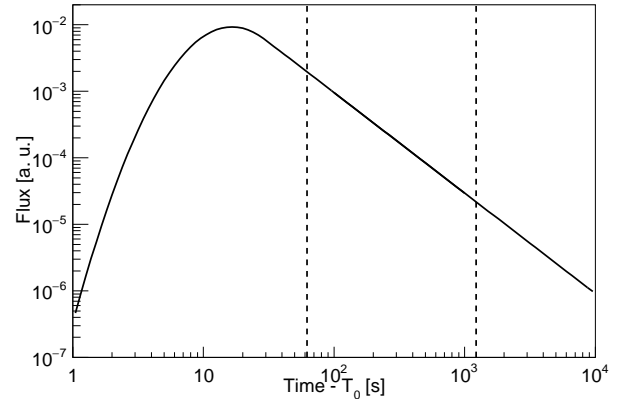


FIG. 1: Intrinsic LC model. The full line represents the LC reported in [21]. The vertical dashed lines represent the bounds of the time interval considered in our analysis.

cal considerations. The light curve (LC) model is shown in Fig. 1. For the purposes of this study, we parametrized the LC for the duration of the observation as follows:

$$\Phi_2(t) \propto \begin{cases} 0 & t < T_0 \equiv 0 \\ h(t) & T_0 < t < T_1 \\ h(T_1) T_1^\beta t^{-\beta} & t > T_1 \end{cases} \quad (7)$$

where $h(t) = t^{7.3-1.3 \ln(t)}$ and $T_1 = 30$ s [21].

For our LIV analysis, we selected events recorded during the first 19 minutes of observation of GRB 190114C, with stable observational conditions and covering approximately 90% of all observed events. The signal events were extracted from the so-called ON region, a circular sky region of radius $0.1^\circ - 0.2^\circ$ (depending on the energy) around the position of the source, which also contains background events. The background content of the ON region was estimated counting events in three simultaneous OFF regions of the same size as the ON region. This resulted in a total of $N_{\text{ON}} = 726$ and $N_{\text{OFF}} = 119$ events (i.e., $119/3 = 39.67$ estimated background events in the ON region), with estimated energies from $E_{\text{min}} = 300$ GeV to $E_{\text{max}} = 1955$ GeV and arrival times from $t_{\text{min}} = 62$ s to $t_{\text{max}} = 1212$ s after T_0 .

III. MAXIMUM LIKELIHOOD ANALYSIS

We use the maximum likelihood method to estimate the value of the LIV parameter η_n ($n \in \{1, 2\}$). It was first employed in ToF studies of LIV using Cherenkov telescopes in [24]. The likelihood function is comprised of probability distribution functions (PDF) of the estimated energy and the arrival time of individual photons. The PDF depends on:

- The assumptions “ I ” on the intrinsic properties of

the source, e.g., the parameters of the intrinsic energy and temporal photon distributions,

- The LIV effects we are interested to explore, i.e., the parameter η_n introduced in Sec. I,
- Other photon propagation effects. Specifically, VHE γ rays are partially absorbed by the extragalactic background light (EBL, see, e.g., [25]), resulting in the observed spectrum being softer compared to the intrinsic one,
- The instrument response functions.

We assume that the intrinsic energy and temporal distributions are independent, i.e., $\Phi(E, t) = \Phi_1(E) \Phi_2(t)$. The PDF for detecting a signal event of a given estimated energy E_{est} at a time t is

$$f_s(t, E_{\text{est}} | \eta_n, I) \propto \int_0^\infty dE \Phi_1(E) \Phi_2(t - \Delta t(E, \eta_n)) \times F(E) A_{\text{eff}}(E) G(E_{\text{est}}, E), \quad (8)$$

where:

- $F(E)$ is the EBL attenuation, which in this work we computed using the model of A. Domínguez et al. [25] with $z = 0.4245$.
- $A_{\text{eff}}(E)$ and $G(E_{\text{est}}, E)$ are, respectively, the effective area and PDF of the energy estimator for photons of true energy E , obtained from Monte Carlo simulations.

The intrinsic energy distribution is modeled with a power law as described in Sec. II. Energy dependent ToF implies that photons of different energies detected at the same time were emitted at different times. For large enough time delays, the emission time will not be within the MAGIC observation window. In addition, the temporal distribution in the MAGIC observation window shows

a limited variability with a monotonic decay, while the flux peak is preceding the MAGIC observations. Inability to set strong constraints on the emission time limits our analysis sensitivity. Therefore, we need to make an assumption on the shape of the intrinsic temporal distribution of γ -rays beyond the interval of MAGIC observations. For this, we adopt the following two approaches:

1. In the *minimal* approach our only assumption is that the γ -ray emission started at T_0 , and we avoid making any further assumptions about the temporal distribution of the photons. Therefore, we define the time model as a step function:

$$\Phi_2(t) = \begin{cases} 0 & t < T_0, \\ k & t \geq T_0, \end{cases} \quad (9)$$

where k is an arbitrary constant absorbed in the PDF normalization. Any event has equal probability of being emitted at any time after T_0 , thus avoiding any assumption about the intrinsic temporal photon distribution. Because of the form of the LC model, this approach only allows us to set an upper limit on the value of η_n . Note that in the absence of background and for perfect energy resolution, using this model would yield $\mathcal{L} = 0$ for η above the value implying that at least one of the observed photons would have been emitted before T_0 (as done in [26]). In this sense the approach is conservative, since the only assumption is that there was no γ -ray emission before T_0 .

2. In the *theoretical* approach, we adopt the intrinsic temporal distribution as parametrized in Eq. (7) and shown in Fig. 1, i.e., we fully adopt the LC model from [21].

In both approaches, all 726 events from the ON region are used for the likelihood maximization. The intrinsic parameters α and β are treated as nuisance parameters, the latter one being only applicable for the theoretical approach. Finally, the likelihood function can be written as

$$\mathcal{L} \left(\eta_n; I | \{t^{(i)}, E_{\text{est}}^{(i)}\}_{i=1, \dots, N_{\text{ON}}}, N_{\text{ON}}, N_{\text{OFF}} \right) = P(I) \times \times \prod_i^{N_{\text{ON}}} \left(\frac{N_{\text{ON}} - N_{\text{OFF}}/\tau}{N_{\text{ON}}} \frac{f_s(t^{(i)}, E_{\text{est}}^{(i)} | \eta_n, I)}{\int_{E_{\text{min}}}^{E_{\text{max}}} dE_{\text{est}} \int_{t_{\text{min}}}^{t_{\text{max}}} dt f_s(t, E_{\text{est}} | \eta_n, I)} + \frac{N_{\text{OFF}}}{\tau N_{\text{ON}}} \frac{f_b(t^{(i)}, E_{\text{est}}^{(i)})}{\int_{E_{\text{min}}}^{E_{\text{max}}} dE_{\text{est}} \int_{t_{\text{min}}}^{t_{\text{max}}} dt f_b(t, E_{\text{est}})} \right), \quad (10)$$

where $E_{\text{est}}^{(i)}$ and $t^{(i)}$ are the estimated energy and arrival time, respectively, of event i . $P(I)$ is the PDF of the parameters describing the intrinsic energy and temporal evolution of the source. For the theoretical approach, we assume that α and β are distributed according to normal

distributions centered respectively at -2.5 and -1.51 , with standard deviations 0.2 and 0.04 , respectively [21]. τ is the ratio of exposure time between the background and the signal regions. In our case $\tau = 3$ (see Section II). The background PDF $f_b(t, E_{\text{est}})$ is obtained assum-

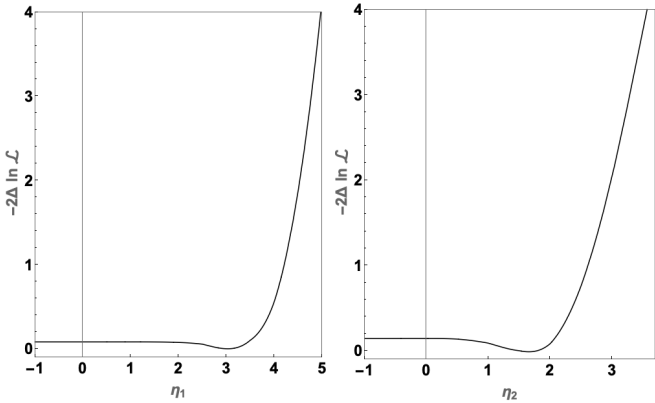


FIG. 2: Likelihood profile for the linear (left) and quadratic (right) case, using the minimal model for the intrinsic LC.

ing a uniform distribution in time (justified by the stable observation conditions), while for estimating the energy distribution we use events collected with MAGIC when pointing under the same observational conditions to regions of the sky with no known γ -ray sources.

We then compute

$$-2\Delta \ln(\mathcal{L}) = -2 \ln \left(\frac{\max(\mathcal{L})_I}{\max(\mathcal{L})_{\eta_n, I}} \right) \quad (11)$$

as a function of η_n . In Eq. 11 we have introduced the notation $\max(\mathcal{L})_I \equiv \mathcal{L}(x, \hat{I})$ where \hat{I} maximizes \mathcal{L} for a given value of x . In this way we treat all the intrinsic parameters in the maximum likelihood as nuisance parameters. This approach has the advantage that uncertainties on the intrinsic properties of the source (namely the spectral index α and the index β of the integral flux power-law decay defined in Eq. 7) are included in the obtained confidence intervals (CIs) for the QG energy scale.

IV. RESULTS AND DISCUSSION

The results for $-2\Delta \ln \mathcal{L}$ vs. η_n for the linear and quadratic modification and for the two assumed intrinsic LC models described in Sec. III are shown in Fig. 2 (minimal model) and Fig. 3 (theoretical model). As expected, the minimal LC model yields a constant likelihood value (despite small fluctuation) up to $\eta_1 \simeq 3.5$ for the linear, and $\eta_2 \simeq 2.1$ for the quadratic modification, after which the likelihood values rapidly decrease. Larger values of η would imply that some of the observed events should have been emitted before T_0 . For instance, for the linear case and $\eta_1 = 5$, we expect a delay of ~ 83 s for γ rays of $E = 1$ TeV, whereas we have observed an $E_{\text{est}} = 1.07$ TeV event at $t = 73.6$ s. Using the theoretical temporal distribution, we find that the likelihood is maximal for the “uncalibrated” values $\eta_1 = -1.6$ for the linear case, and $\eta_2 = -1.32$ for the quadratic case. In order to obtain

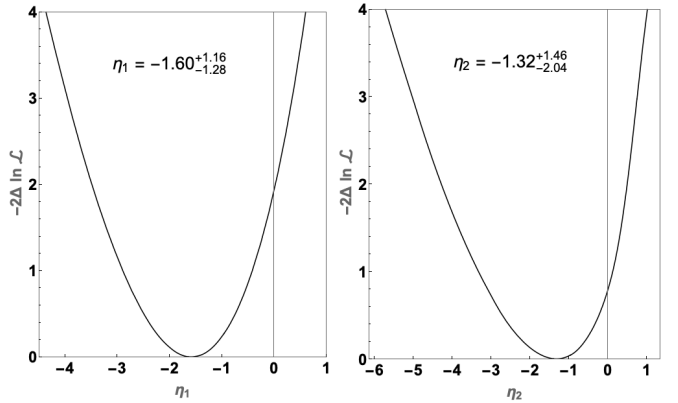


FIG. 3: Likelihood profile for the linear (left) and quadratic (right) case, using the theoretical model for the intrinsic LC.

“calibrated” estimators for η (and “calibrated” CIs, see below), we evaluate the PDF of the η estimator for the null hypothesis ($\eta = 0$) and subtract the observed bias, i.e., the mean of such PDF. Note that, when building the likelihood function, we have assumed certain spectral and temporal distributions for the signal events, which we cannot be sure are the true ones (we actually measured them with our data, only up to a certain precision and under several theoretical assumptions [17, 21]). Because of this, we cannot presume the validity of the Wilks theorem, i.e., that the PDF for $-2\Delta \ln \mathcal{L}$ is a χ^2 with one degree of freedom, or that the estimator of η distributes as a Gaussian around the true value η_{true} . Thus, to evaluate the PDF of the η estimator we apply the maximum likelihood method to 1000 mock data sets. Each of them is generated starting from the measured data set, first “reshuffling” the event arrival times, and then applying once the bootstrapping resampling technique. Reshuffling consists of reassigning randomly the measured arrival times to the different observed events, which has the effect of removing any energy-time correlation present in the data (in particular, any LIV effect), without altering the overall spectral and temporal distributions of the signal. Bootstrapping creates samples of the same size by randomly selecting events (repetition is allowed) from the original data set, and therefore allows the measured spectral and temporal distributions to vary within their natural statistical uncertainties. By maximizing the likelihood for each of the reshuffled-bootstrapped samples and making the histogram of the resulting best fits we determine the PDF of our estimator, whose mean is the bias η_{bias} of our analysis (see Fig. 4). From this PDF we determine the p -value of the null hypothesis, i.e., the significance of the detection of a LIV effect, as its integral above $\eta_{\text{uncal.}}$ and below $2\eta_{\text{bias}} - \eta_{\text{uncal.}}$. Our results for the theoretical LC, $p_{\eta_1} = 0.78$ and $p_{\eta_2} = 0.59$, are consistent with the null hypothesis. For the theoretical LC we obtain $\eta_{1,\text{bias}} = -1.9$ and $\eta_{2,\text{bias}} = -2.6$, respectively. The “calibrated” best-fit values for η are then

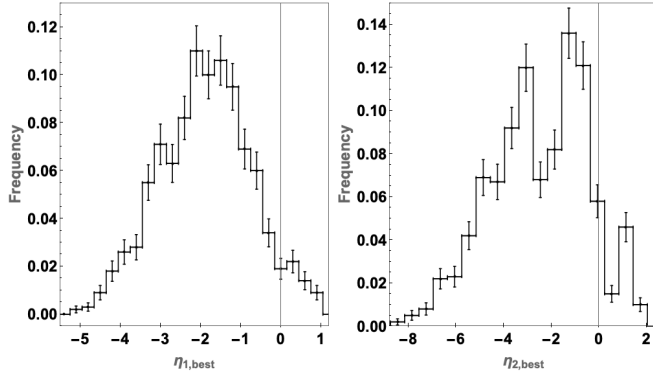


FIG. 4: Distribution of best fits of η_1 (linear case, left) and η_2 (quadratic case, right), obtained from reshuffled-bootstrapped samples and using the theoretical assumption for the intrinsic LC.

obtained as $\eta_{\text{best}} = \eta_{\text{uncal.}} - \eta_{\text{bias}}$, with the numerical values shown in Table I. Note that this procedure is not applicable to the minimal LC, for which the bias is not well-defined, and which is valid by construction only to obtain robust model-independent upper limits to η . Also note that a more standard definition of the calibrated best-fit η would be the true value of η for which the mean of the corresponding PDF of the maximum likelihood estimator is equal to the observed $\eta_{\text{uncal.}}$. However, in order to follow this procedure, we would need to rely on Monte Carlo simulations to produce our mock data sample for non-null true η values, which is not feasible because, as mentioned above, we do not know the true spectral and temporal distributions needed for the generation. However, both methods should produce identical results provided that η_{bias} does not depend on the true value of η .

Finally, we construct calibrated 95% CIs from the reshuffled-bootstrapped samples, following the procedure from [11]. Since the PDF of $-2\Delta \ln \mathcal{L}$ is not a χ^2 distribution, we cannot rely on the standard technique of finding the values of η for which $-2\Delta \ln \mathcal{L}$ reaches the 3.8 threshold. Instead, we build the PDF of the values of η corresponding to different values of the $-2\Delta \ln \mathcal{L}$ threshold and find the threshold for which the quantile of the PDF below (above) η_{bias} is 2.5% (see Fig. 5). The “uncalibrated” upper (lower) limit $\eta_{\text{uncal.}}^{\text{UL}}$ ($\eta_{\text{uncal.}}^{\text{LL}}$) is then determined in the usual way from the observed $-2\Delta \ln \mathcal{L}$ vs. η curve but using the obtained threshold. Finally, we compute the fully calibrated upper (lower) limits as $\eta^{\text{UL}} = \eta_{\text{uncal.}}^{\text{UL}} - \eta_{\text{bias}}$ ($\eta^{\text{LL}} = \eta_{\text{uncal.}}^{\text{LL}} - \eta_{\text{bias}}$). This procedure differs again from the standard Neyman construction of CIs, which is not feasible because it requires Monte Carlo simulations, but should produce equal results provided the PDF for $\eta - \eta_{\text{true}}$ is symmetric with respect to its mean, and does not depend on η_{true} . The obtained calibrated CIs are reported in Table I (assuming $\eta_{\text{bias}} = 0$ in the case of the minimal LC). Finally, using Eq. 4 and 5, these values are translated into the

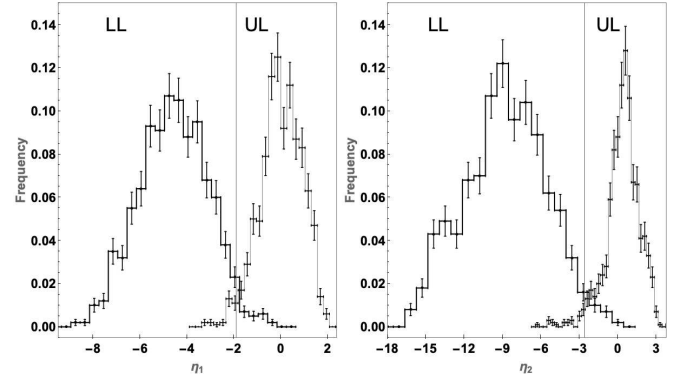


FIG. 5: Distribution of lower (thick line) and upper limits (thin line) for the linear (left) and quadratic case (right), obtained from reshuffled-bootstrapped samples and using the theoretical assumption for the intrinsic LC. The vertical lines indicate respective bias values.

limits on the energy scale E_{QG} at 95% confidence level and reported in Table I.

TABLE I: Values of the 95% lower (LL) and upper (UL) limits and the best fits (BF) obtained for η_n using the theoretical intrinsic LC model, after applying bias correction and CI calibration. Only upper limits can be set with the minimal approach (see text). Values are reported for the linear ($n = 1$) and quadratic ($n = 2$) cases.

LC model	Minimal (step function)	Theoretical ([21])		
	η^{UL}	η^{LL}	η^{BF}	η^{UL}
η_1	4.4	-2.2	0.3	2.1
η_2	2.8	-4.8	1.3	3.7
	subl.	superl.		subl.
$E_{\text{QG},1} [10^{19} \text{ GeV}]$	0.28	0.55		0.58
$E_{\text{QG},2} [10^{10} \text{ GeV}]$	7.3	5.6		6.3

A possible change of spectral index of GRB 190114C with time was reported in [21]. We inspected the resulting systematic effect on η , and found that it is less than 5% in all cases. Additionally, using a dedicated study with Monte Carlo simulations, we computed that the limits would degrade by up to 18% (29%) in subluminal (superluminal) cases, should the Cherenkov light collected by the telescopes be overestimated by 15% in our analysis, which is a conservative assumption.

V. CONCLUSIONS AND SUMMARY

MAGIC discovered a γ -ray signal above 0.2 TeV from GRB 190114C, detecting the highest energy photons from a GRB. Using conservative assumptions on the intrinsic spectral and temporal emission properties, we searched for an energy-dependent delay in arrival time of the most

energetic photons, testing in vacuo dispersion relations of VHE photons. We assumed two different models for the LC: minimal and theoretical, described in detail in Sec. III. In both cases, our results are compatible with the null hypothesis of no time delay. We were able to set lower limits on QG LIV energy scale. Our results for the linear modification of the photon dispersion relation $E_{QG,1} > 0.58 \times 10^{19}$ GeV ($E_{QG,1} > 0.55 \times 10^{19}$ GeV) for the subluminal (superluminal) case are approximately a factor 4 (7) below the most constraining lower limits on $E_{QG,1}$ obtained from ToF method on GRB 090510 [11]. This is expected because of a significantly larger distance of GRB 090510 ($z = 0.9$, compared to 0.4245 of GRB 190114C), as well as a shorter variability timescale, since *Fermi*-LAT observations of GRB 090510 include a full coverage of the emission. In the case of the quadratic modification of the dispersion relation, the analysis is more sensitive to the highest photon energies in the data sample (estimated $E_{\max} = 1955$ GeV, compared to $E_{\max} = 31$ GeV for GRB 090510 [11]). As a result, our lower limits on the energy scale $E_{QG,2} > 6.3 \times 10^{10}$ GeV ($E_{QG,2} > 5.6 \times 10^{10}$ GeV) for the subluminal (superluminal) case are more constraining than the ones in [11]. At the same time, our results for the quadratic case are comparable to the ones from [12]. GRB 190114C is at redshift more than one order of magnitude higher than Mrk 501, however measured spectrum in Mrk 501 data reaches an order of magnitude higher energies [12], resulting in comparable sensitivities. It is worth noting that MAGIC observed a featureless afterglow phase of the GRB 190114C, limiting the sensitivity of our LIV analysis. We are looking forward to VHE observations of an expectedly feature-rich GRB prompt phase, which would enhance the analysis sensitivity to LIV effects.

ACKNOWLEDGMENTS

We would like to thank the Instituto de Astrofísica de Canarias for the excellent working conditions at

the Observatorio del Roque de los Muchachos in La Palma. The financial support of the German BMBF and MPG, the Italian INFN and INAF, the Swiss National Fund SNF, the ERDF under the Spanish MINECO (FPA2017-87859-P, FPA2017-85668-P, FPA2017-82729-C6-2-R, FPA2017-82729-C6-6-R, FPA2017-82729-C6-5-R, AYA2015-71042-P, AYA2016-76012-C3-1-P, ESP2017-87055-C2-2-P, FPA201790566REDC), the Indian Department of Atomic Energy, the Japanese JSPS and MEXT, the Bulgarian Ministry of Education and Science, National RI Roadmap Project DO1-153/28.08.2018 and the Academy of Finland grant nr. 320045 is gratefully acknowledged. This work was also supported by the Spanish Centro de Excelencia “Severo Ochoa” SEV-2016-0588 and SEV-2015-0548, and Unidad de Excelencia “María de Maeztu” MDM-2014-0369, by the Croatian Science Foundation (HrZZ) Project IP-2016-06-9782 and the University of Rijeka Project 13.12.1.3.02, by the DFG Collaborative Research Centers SFB823/C4 and SFB876/C3, the Polish National Research Centre grant UMO-2016/22/M/ST9/00382 and by the Brazilian MCTIC, CNPq and FAPERJ. This project has received funding from the Foundation Blanceflor Boncompagni Ludovisi, née Bildt. This project has received funding from the European Union’s Horizon 2020 research and innovation programme under the Marie Skłodowska-Curie grant agreement No. 754510. L. Nava acknowledges funding from the European Unions Horizon 2020 Research and Innovation programme under the Marie Skłodowska-Curie grant agreement n. 664931

[1] V. A. Kostelecký and S. Samuel, Spontaneous breaking of lorentz symmetry in string theory, *Phys. Rev. D* **39**, 683 (1989).

[2] G. Amelino-Camelia, J. Ellis, N. E. Mavromatos, D. V. Nanopoulos, and S. Sarkar, Tests of quantum gravity from observations of γ -ray bursts, *Nature* **393**, 763 (1998).

[3] R. Gambini and J. Pullin, Nonstandard optics from quantum space-time, *Phys. Rev. D* **59**, 124021 (1999).

[4] S. M. Carroll, J. A. Harvey, V. A. Kostelecký, C. D. Lane, and T. Okamoto, Noncommutative Field Theory and Lorentz Violation, *Phys. Rev. Lett.* **87**, 141601 (2001).

[5] J. Lukierski, H. Ruegg, and W. J. Zakrzewski, Classical and Quantum Mechanics of Free κ -Relativistic Systems, *Annals of Physics* **243**, 90 (1995).

[6] G. Amelino-Camelia and S. Majid, Waves on Non-commutative Space-Time and Gamma-Ray Bursts, *International Journal of Modern Physics A* **15**, 4301 (2000).

[7] C. P. Burgess, J. M. Cline, E. Filotas, J. Matias, and G. D. Moore, Loop-generated bounds on changes to the graviton dispersion relation, *Journal of High Energy Physics* **2002**, 043 (2002).

[8] T. Kifune, Invariance Violation Extends the Cosmic-Ray Horizon?, *The Astrophysical Journal* **518**, L21 (1999).

[9] U. Jacob and T. Piran, Lorentz-violation-induced arrival delays of cosmological particles, *Journal of Cosmology and Astroparticle Physics* **2008**, 031 (2008).

[10] W. B. Atwood *et al.* (*Fermi*-LAT Collaboration), The Large Area Telescope on the *Fermi* Gamma-Ray Space Telescope Mission, *The Astrophysical Journal* **697**, 1071 (2009).

[11] V. Vasileiou, A. Jacholkowska, F. Piron, J. Bolmont, C. Couturier, J. Granot, F. W. Stecker, J. Cohen-Tanugi, and F. Longo, Constraints on Lorentz invariance violation from Fermi-Large Area Telescope observations of gamma-ray bursts, *Phys. Rev. D* **87**, 122001 (2013).

[12] H. Abdalla *et al.* (H.E.S.S. Collaboration), The 2014 TeV γ -Ray Flare of Mrk 501 Seen with H.E.S.S.: Temporal and Spectral Constraints on Lorentz Invariance Violation, *Astrophys. J.* **870**, 93 (2019).

[13] M. L. Ahnen *et al.* (MAGIC Collaboration), Constraining Lorentz Invariance Violation Using the Crab Pulsar Emission Observed up to TeV Energies by MAGIC, *ApJS* **232**, 9 (2017).

[14] M. Ajello *et al.* (*Fermi*-LAT Collaboration), A Decade of Gamma-Ray Bursts Observed by Fermi-LAT: The Second GRB Catalog, *Astrophys. J.* **878**, 52 (2019).

[15] J. Selsing, J. P. U. Fynbo, K. E. Heintz, and D. Watson, GRB 190114C: NOT optical counterpart and redshift., *GRB Coordinates Network* **23695**, 1 (2019).

[16] A. J. Castro-Tirado, Y. Hu, E. Fernandez-Garcia, A. Valeev, V. Sokolov, S. Guziy, S. Oates, S. Jeong, S. B. Pandey, I. Carrasco, and D. Reverte-Paya, GRB 190114C: refined redshift by the 10.4m GTC., *GRB Coordinates Network* **23708**, 1 (2019).

[17] V. A. Acciari *et al.* (MAGIC Collaboration), Teraelectronvolt emission from the γ -ray burst GRB 190114C, *Nature* **575**, 455 (2019).

[18] J. Aleksić *et al.* (MAGIC Collaboration), The major upgrade of the MAGIC telescopes, Part I: The hardware improvements and the commissioning of the system, *Astroparticle Physics* **72**, 61 (2016).

[19] J. D. Gropp, J. A. Kennea, N. J. Klingler, H. A. Krimm, S. J. Laporte, A. Y. Lien, M. J. Moss, D. M. Palmer, B. Sbarufatti, and M. H. Siegel, GRB 190114C: Swift detection of a very bright burst with a bright optical counterpart., *GRB Coordinates Network* **23688**, 1 (2019).

[20] R. Hamburg, P. Veres, C. Meegan, E. Burns, V. Connaughton, A. Goldstein, D. Kocevski, and O. J. Roberts, GRB 190114C: Fermi GBM detection., *GRB Coordinates Network* **23707**, 1 (2019).

[21] V. A. Acciari *et al.* (MAGIC Collaboration), Observation of inverse Compton emission from a long γ -ray burst, *Nature* **575**, 459 (2019).

[22] R. Zanin *et al.* (MAGIC Collaboration), MARS, the MAGIC analysis and reconstruction software, in *Proceedings of the 33rd ICRC* (2013) p. 0773.

[23] J. Aleksić *et al.* (MAGIC Collaboration), The major upgrade of the MAGIC telescopes, Part II: A performance study using observations of the Crab Nebula, *Astroparticle Physics* **72**, 76 (2016).

[24] M. Martínez and M. Errando, A new approach to study energy-dependent arrival delays on photons from astrophysical sources, *Astroparticle Physics* **31**, 226 (2009).

[25] A. Domínguez, J. R. Primack, D. J. Rosario, F. Prada, R. C. Gilmore, S. M. Faber, D. C. Koo, R. S. Somerville, M. A. Prez-Torres, P. Prez-González, J.-S. Huang, M. Davis, P. Guhathakurta, P. Barmby, C. J. Conselice, M. Lozano, J. A. Newman, and M. C. Cooper, Extragalactic background light inferred from aegis galaxy-sed-type fractions, *MNRAS* **410**, 2556 (2011).

[26] A. A. Abdo *et al.* (*Fermi*-GBM/LAT Collaborations), A limit on the variation of the speed of light arising from quantum gravity effects, *Nature* **462**, 331 EP (2009).